

# A FAST METHOD FOR THE PREDICTION OF DYNAMIC STALL ONSET ON TURBOMACHINERY BLADES

K. D. Jones<sup>†</sup> and M. F. Platzer<sup>‡</sup>

Naval Postgraduate School  
Monterey, California

## Abstract

A computational approach is described for the rapid and systematic prediction and evaluation of the onset of dynamic stall due to rapid incidence changes or unsteady pitch or plunge motions. The method combines an unsteady, two-dimensional panel code with a two-dimensional boundary layer code. The panel code provides incompressible, inviscid flowfields about arbitrary airfoils undergoing prescribed motions. The boundary layer code computes laminar, transitional and turbulent regimes, with transition onset predicted by Michel's criterion. Presented results demonstrate that the delay in dynamic stall onset is directly related to the dynamic pressure lag, in agreement with previous Navier-Stokes simulations, but in apparent disagreement with several aspects of the 'moving wall' analogy suggested in the past as an explanation for delayed dynamic stall onset.

## Nomenclature

$c$	= chord length
$C_p$	= pressure coefficient, $(p - p_\infty)/q_\infty$
$h$	= plunge amplitude in terms of $c$
$k$	= reduced frequency, $2\pi f c/V_\infty$
$p$	= pressure
$q_\infty$	= freestream dynamic pressure, $1/2\rho_\infty V_\infty^2$
$Re_L$	= chord Reynolds number, $V_\infty c/\nu_\infty$
$t$	= time
$U$	= tangent velocity in the boundary layer
$U_e$	= boundary layer edge velocity
$V_\infty$	= freestream velocity
$x_p$	= chordwise pivot location
$z(\tau)$	= plunge displacement, positive downward
$\alpha$	= angle of attack, positive clockwise
$\phi$	= phase angle between pitch and plunge
$\nu_\infty$	= freestream kinematic viscosity
$\rho_\infty$	= freestream density
$\tau$	= nondimensional time, $tV_\infty/c$

---

<sup>†</sup> NRC Research Associate

<sup>‡</sup> Professor, Fellow, ASME

This paper is declared a work of the U.S. Government and is not subject to copyright protection in the United States.

## Introduction

The problem of the onset of flow separation on airfoils due to rapid incidence changes or unsteady motions is a problem of continuing fundamental and applied interest. In the past, two major approaches have been used to predict the onset of dynamic airfoil stall; semi-empirical and Navier-Stokes methods. Examples of semi-empirical approaches are those of Ericsson,<sup>1</sup> Tyler and Leishman<sup>2</sup> and Beddoes,<sup>3</sup> among others. On the other hand, recent advances in computational fluid dynamics have stimulated the 'brute force' computation of dynamic stall by solving the Navier-Stokes equations. Unfortunately, both approaches have serious deficiencies which affect their predictive capabilities.

The physical flow models and the mathematical simplifications used in the semi-empirical approaches are rather severe and, therefore, require the introduction of additional empirical information in order to 'calibrate' the models to achieve agreement with the available experimental data. The generalization of the semi-empirical methods to new cases therefore entails considerable uncertainties.

The brute-force Navier-Stokes computations, on the other hand, introduce another set of uncertainties because the solutions require the use of the Reynolds-averaged equations and, therefore, the use of turbulence models to achieve closure of the equations. As shown by Dindar et al,<sup>4</sup> Visbal,<sup>5</sup> and Clarkson et al,<sup>6</sup> different turbulence models produce substantially different dynamic stall hysteresis loops. Furthermore, most Navier-Stokes calculations are performed by assuming the flow to be either fully laminar or fully turbulent. Recently, Ekaterinaris and Platzer<sup>7</sup> showed that it is crucial to include a proper transition model in order to obtain improved agreement with available experiments. Hence, the development of a satisfactory dynamic stall prediction method requires a continuing sustained effort in order to better understand the important physical and computational aspects required for the modeling of this complicated flow phenomenon.

In the present paper we take an approach which is intended to bridge the gap between the semi-empirical approaches and the Navier-Stokes solutions. We

limit ourselves to low-speed flows and hence make the assumption that the analysis can be based on incompressible flow methods. Furthermore, we limit ourselves to the analysis of the *onset* of dynamic stall. For many airfoils the dynamic stall process is initiated by the formation of a separation bubble near the airfoil leading edge at a relatively low angle of attack. The bubble is formed when separation occurs in the laminar flow region of the boundary layer, and the disturbance caused by the separation triggers transition to turbulent flow. The transitional flow introduces energy into the boundary layer, causing the boundary layer to re-attach. In such cases, predicting the onset of dynamic stall becomes a problem of predicting laminar separation.

Evidence was presented in Grohsmeyer et al<sup>8</sup> that the onset of dynamic stall occurred when a critical pressure gradient distribution was reached, and that this critical distribution was essentially independent of the pitch rate and Mach number.

In the present study an unsteady panel code is combined with a boundary layer code to compute unsteady, incompressible, two-dimensional, viscous flows. The hybrid code allows the rapid and precise computation of the pressure distribution and pressure lag effect due to oscillation mode, frequency and amplitude, as well as the dependence on airfoil geometry.

The Keller-Cebeci finite-difference box method is coupled with the unsteady panel code in order to study the detailed changes in the boundary layer behavior up to incipient separation as a function of mode and frequency of oscillation. These computational results make it possible to evaluate the validity of previously suggested flow models, such as Ericsson's *moving wall* or leading edge jet effect, and to investigate the dependence of dynamic stall onset on the surface pressure distribution.

## Approach

The numerical methods utilized in the panel code and the boundary layer code are briefly summarized in the following subsections, with details and validations of the methods available in the cited references.

**Panel Code** Flow solutions are computed using an unsteady, potential-flow code originally developed by Teng.<sup>9</sup> The basic, steady panel code follows the approach of Hess and Smith,<sup>10</sup> where the airfoil is approximated by a finite number of panels, each with a local, uniform, distributed source strength and all with a global, uniform, distributed vorticity strength. For  $n$  panels there are  $n$  unknown source strengths,  $q_j$ , and an unknown vorticity strength,  $\gamma$ . Boundary conditions include flow tangency at the midpoint of the  $n$

panels and the Kutta condition which postulates that the pressure on the upper and lower surfaces of the airfoil at the trailing edge must be equal.

The unsteady panel code adopts the procedure of Basu and Hancock,<sup>11</sup> where a wake panel is attached to the trailing edge through which vorticity is shed into the flow, as shown in Fig. 1. The Helmholtz theorem states that the bound vorticity in a flow remains constant, thus a change in circulation about the airfoil must result in the release of vorticity into the wake equal in magnitude and opposite in direction, given numerically by

$$\Delta_k(\gamma_w)_k + \Gamma_k = \Gamma_{k-1} \quad (1)$$

where  $\Delta$  is the wake panel length,  $\gamma_w$  is the distributed vorticity strength on the wake panel and  $\Gamma$  is the circulation about the airfoil, and where the subscript  $k$  indicates the current time step, and  $k-1$  indicates the previous time step.

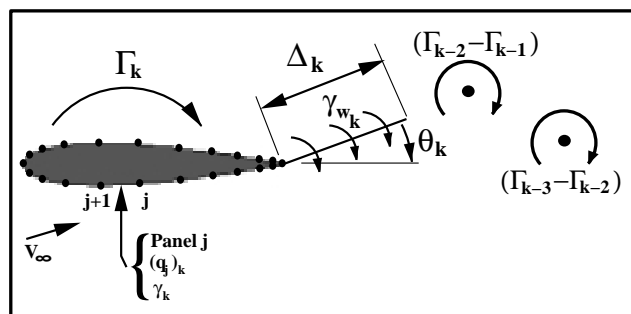


**Fig. 1:** Schematic of the panel code wake model.

The wake panel introduces two additional unknowns; the wake panel length and its orientation,  $\theta_k$ . Thus, two additional conditions must be specified for closure;

1. The wake panel is oriented in the direction of the local resultant velocity at the panel midpoint.
2. The length of the wake panel is proportional to the magnitude of the local resultant velocity at the panel midpoint and the time-step size.

At the end of each time step the vorticity contained in the wake panel is concentrated into a point vortex which is shed into the wake and convected downstream with the flow, influencing and being influenced by the other shed vortices and the airfoil. Note, implementation of this approach requires an iterative scheme, since the velocity direction and magnitude used to define the wake panel are not initially known. Note also that this wake model is nonlinear. The unsteady panel code has been extensively documented in Refs. 9 and 12-17.

**Boundary Layer Code** Flow properties in the boundary layer are computed using the Keller-Cebeci

box method.<sup>18</sup> The code was generated and combined with a steady panel code by Nowak.<sup>19</sup> The general algorithm and several modifications used in the current implementation are discussed below.

The boundary layer code treats the airfoil surface as a flat plate with a variable pressure gradient, and steady conditions are assumed within the boundary layer. Laminar, transitional and turbulent regions are considered, and the turbulent region is computed using the Cebeci-Smith (CS) eddy-viscosity model. Like all eddy-viscosity methods, the CS model leaves the basic boundary layer equations unchanged but modifies the viscosity term by adding a local eddy viscosity,  $\nu = \nu_\infty + \epsilon_m$ . The CS model divides the viscous region into an inner and an outer layer with the eddy viscosity in each region empirically formulated. The inner region is modeled by

$$\left(\frac{\epsilon_m}{\nu}\right)_i = 0.16\sqrt{Re_x} \left[1 - \exp(-y/A)\right]^2 \eta^2 \nu_\infty \gamma_{tr} \quad (2)$$

and the outer region is modeled by

$$\left(\frac{\epsilon_m}{\nu}\right)_o = 0.0168\sqrt{Re_x} \left[\eta_e - f_e\right] \gamma_{tr} \quad (3)$$

where

$$Re_x = \frac{U_e}{V_\infty} \xi R_L \quad (4)$$

$$\frac{y}{A} = \frac{\eta}{26} \sqrt[4]{Re_x} \sqrt{\nu_w} \quad (5)$$

and where  $\xi$ ,  $\eta$  and  $f$  are the Falkner-Skan variables. The term  $\gamma_{tr}$  models the length of the transition or intermittency region, and its formulation is discussed below.

The point of transition onset is of critical importance for the prediction of dynamic stall. For the steady implementation of the code developed by Nowak the transition point is specified as input, presumably determined from experimental data. This is of little use in the present unsteady approach, as transition points would need to be specified for an infinite variety of conditions. Thus Michel's criterion is used to predict transition onset, where transition is initiated when the Reynolds number based on momentum thickness,  $R_\theta$ , and the Reynolds number based on  $x$ ,  $Re_x$ , satisfy the equation

$$R_{\theta_{tr}} = 1.174 \left(1 + \frac{22,400}{Re_{x_{tr}}}\right) Re_{x_{tr}}^{0.46} \quad (6)$$

where  $R_\theta = U_e \theta / \nu_\infty$ .

The Chen-Thysson intermittency model is used to predict the transition length where

$$\gamma_{tr} = 1 - \exp \left[ -G(x - x_{tr}) \int_{x_{tr}}^x \frac{1}{U_e} dx \right] \quad (7)$$

and

$$G = \frac{1}{G_{tr}} \left(\frac{U_e}{V_\infty}\right)^3 R_L^2 Re_{x_{tr}}^{-1.34} \quad (8)$$

In the original Chen-Thysson formulation  $G_{tr}$  is set to a constant value of 1200, but in the present implementation it is given by Cebeci<sup>20</sup> as a function of the transition Reynolds number

$$G_{tr} = 71 \left[ \ln(Re_{x_{tr}}) - 4.732 \right] \quad (9)$$

The use of Michel's criterion for the prediction of transition onset and the use of the Chen-Thysson model for the transition region has been validated in Refs. 20 and 21.

Note, that while the boundary layer routine is steady, it has been shown that, for low reduced frequencies, changes in the boundary layer occur much more quickly than changes in the external flow, thus a steady boundary layer analysis is sufficient.<sup>22</sup>

The present combination of panel and boundary layer codes is not an inviscid/viscous interaction approach (eg. Cebeci et al<sup>23</sup>); that is, information is only passed from the panel code to the boundary layer code; never the other way. Therefore, it is not possible to predict the viscous flow region beyond separation, as the flow separation would have a significant influence on the effective body shape seen by the panel code. However, the hybrid code can be used to predict the point in the cycle and on the airfoil surface where separation first occurs, and by looking in detail at the velocity profiles in the boundary layer, in particular in the region surrounding the suction peak, much insight may be obtained into the initial stages of dynamic stall. Note, the present code runs simulations in a matter of seconds on a workstation, and does not have convergence problems sometimes encountered with inviscid/viscous interaction methods.

## Results

It is important to note that the only information the boundary layer algorithm is given is the surface point distribution and the external velocity distribution computed by the panel code at each time step. From the velocity distribution the local pressure and pressure gradient are computed, and it is really the pressure gradient that determines the nature of the boundary layer. Thus, it is essential to compute the surface pressure distribution accurately, and by looking at the pressure distributions, as well as the predicted position of the stagnation point, much can be

determined about the flowfield without the aid of the boundary layer code.

As an additional consideration, note that in the unsteady panel code the pressure distribution is computed from the unsteady Bernoulli equation and depends on both the local velocity and the time-rate-of-change of the potential. In the boundary layer code this second term is not considered, but for the frequencies of interest in this study the term is negligible.

In Ref. 1 Ericsson introduces the “moving wall” or “leading-edge jet” effect as a mechanism leading to the dynamic-stall lift overshoot. He suggests that for an airfoil pitching upward the leading-edge suction on the upper surface creates fuller, even jet-like boundary layer profiles, delaying dynamic stall, and he further suggests that this phenomenon is similar to the oscillatory Magnus-lift effect present for rotating or translating cylinders. Ericsson’s Fig. 14 from Ref. 1 is duplicated below to illustrate his analogy.

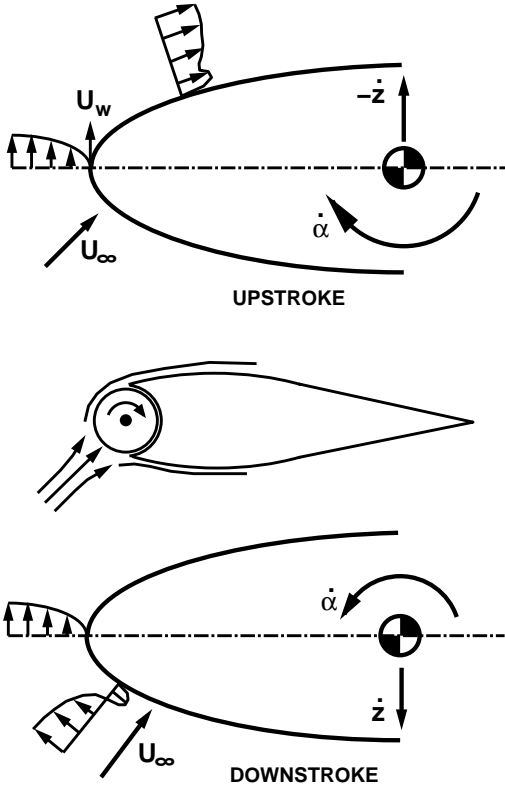


Fig. 2. Ericsson’s Magnus-lift theory.<sup>1</sup>

While slightly fuller (less developed) boundary layer profiles are found for pitching and plunging airfoils (in the vicinity of the suction peak), as shown in Figs. 3 and 4, Ericsson’s analysis of the phenomenon is questionable. In this case the Reynolds number is  $10^6$ , the NACA 0012 airfoil is pitched about its leading edge from 0 to 20 degrees using a modified ramp,

where

$$\alpha(\tau) = \alpha_0 + \Delta\alpha \left[ 10 \left( \frac{\tau}{\tau_c} \right)^3 - 15 \left( \frac{\tau}{\tau_c} \right)^4 + 6 \left( \frac{\tau}{\tau_c} \right)^5 \right] \quad (10)$$

and where

$$\tau_c = \frac{2\pi}{k}, \quad (11)$$

and the presented data is for  $\alpha = 4.53$  degrees at a position 10 percent downstream from the leading edge on the upper surface.

The boundary layer profiles do appear slightly fuller (or less developed) as the pitching frequency is increased, with the largest changes occurring at very low frequencies.

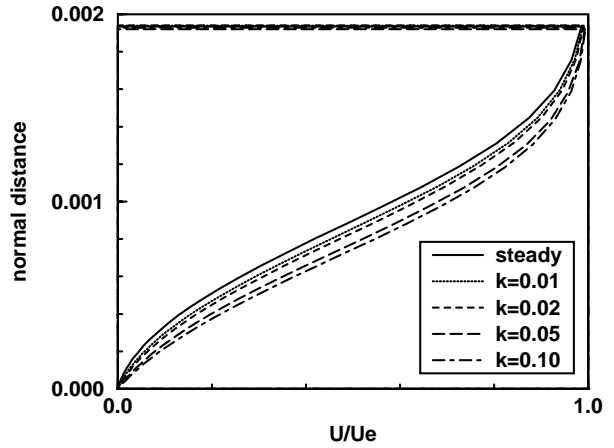


Fig. 3. Boundary layer profiles ( $k = 0.01 - 0.1$ ).

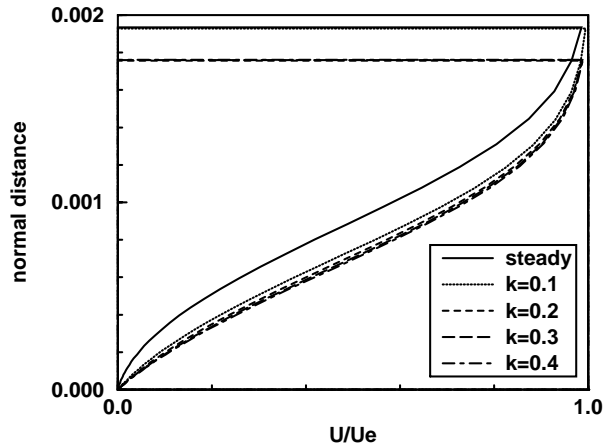


Fig. 4. Boundary layer profiles ( $k = 0.1 - 0.4$ ).

However, we find Ericsson’s moving-wall analogy to be somewhat ill-defined and/or ambiguous. For example, no mention is made of the placement of the pivot location for pitching airfoils, when in fact varying the pivot location is analogous to coupling the pitching motion with an in-phase ( $\phi = 0$  degrees) plunging

motion, where the oscillatory pitching and plunging motions are defined, respectively, by

$$\alpha(\tau) = \alpha_0 + \Delta\alpha \cos(k\tau) , \quad (12)$$

and

$$z(\tau) = -h \cos(k\tau + \phi) . \quad (13)$$

A primary source of confusion arises from Ericsson's Fig. 14, where he suggests that the leading edge jet effect of an airfoil pitching up is equivalent to an airfoil plunging up, and vice versa. First, it is important to keep in mind that plunging a foil with constant velocity is equivalent to an airfoil at a fixed angle of attack (the plunge velocity provides an induced or *effective* angle of attack) and, therefore, to emulate a pitching airfoil, at least with respect to the effective angle of attack, the plunging airfoil must *accelerate*. Thus, it seems inappropriate to compare pitching rate with plunging rate. Second, with reference to the effective angle of attack of a plunging airfoil Ericsson's Fig. 14 would seem to be backward, that is, an airfoil pitching up should be equivalent to an airfoil accelerating down.

The confusion may arise from the indicated pivot location in Ericsson's figures. He shows the foil pivoting about some point downstream of the leading edge, and hence the pitching motion yields an induced, vertical velocity at the leading edge for an airfoil pitching down, similar to that seen by an airfoil plunging down, as illustrated in Fig. 5.

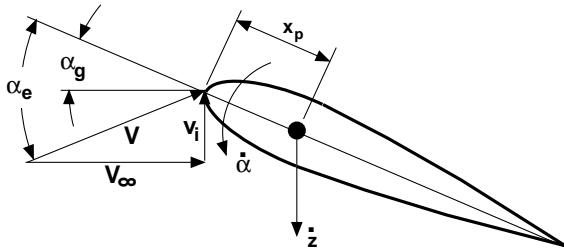


**Fig. 5.** Effective versus geometric  $\alpha$ .

Here the freestream velocity,  $V_\infty$ , and the induced velocity due to plunging and/or pitching,  $v_i$ , combine to yield a total velocity,  $V$ . If the airfoil is at a geometric angle of attack,  $\alpha_g$ , then the induced velocity yields an effective angle of attack,  $\alpha_e$ . However, for pitching airfoils the induced velocity is a local value, dependent on the distance from the pivot location. This variation in the induced velocity, and the resulting variation in the effective angle of attack adds an effective camber to the airfoil.

The effect of varying the pivot location of pitching foils is illustrated in Fig. 6. The boundary layer profiles at a fixed position, roughly 10 percent downstream from the leading edge on the upper surface, are

compared for a NACA 0012 airfoil at a geometric angle of attack of zero degrees for several cases. Included are a steady solution, oscillatory solutions with  $k = 0.1$ ; pitching with  $\Delta\alpha = 5$  degrees and pivot locations of  $x_p = 0$ ,  $x_p = 0.25$  and  $x_p = 0.5$ , and plunging with  $h = 0.0875$ , yielding an effective angle-of-attack range identical to the geometric angle-of-attack range of the pitching foil.

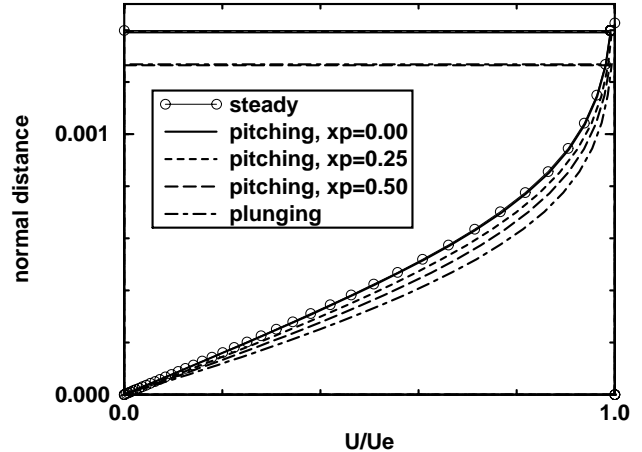


**Fig. 6.** Boundary layer profiles for different modes.

Note that while all 5 cases have a geometric angle of attack of zero degrees, they have different effective angles of attack. Both the steady case and the pitching case with  $x_p = 0$  have an effective angle of attack of zero degrees, and the velocity profiles are almost identical. The pitching case with  $x_p = 0.25$  has an effective angle of attack of -1.25 degrees, the pitching case with  $x_p = 0.5$  has an effective angle of attack of -2.5 degrees, the plunging case has an effective angle of attack of -5.0 degrees, and their velocity profiles get progressively fuller in a seemingly linear relationship with the effective angle of attack. Also note that, due to the variance in the effective angle of attack, there is a similar variance in the position of the stagnation point, and consequently the fuller profiles are also closer to the stagnation point and, logically, less developed.

Comparisons of results for pitching and plunging airfoils should, as a first approximation, be done with the same effective angle of attack, and therefore with  $\phi \approx 90$  degrees. However, as seen in Fig. 6, by moving the pivot location, arbitrary agreement or disagreement of results may be obtained. This is further illustrated in Figs. 7 and 8 by comparing the pressure distributions near the leading edge of a NACA 0012 pitching and plunging. The reduced frequency is 0.1, with  $\Delta\alpha = 10$  degrees for the pitching foil and  $h = 1.76$  and  $\phi = 90$  degrees for the plunging foil.

Note, the indicated angles of attack on Figs. 7

and 8 are the geometric angles of attack for the steady and pitching solutions and the effective angle of attack for the plunging solution. Note also that the pressure lag is consistent throughout the cycle, although it is barely visible at the  $\pm 10$  degree limits (Fig. 7), since the rate of change of the angle of attack is zero at those points.

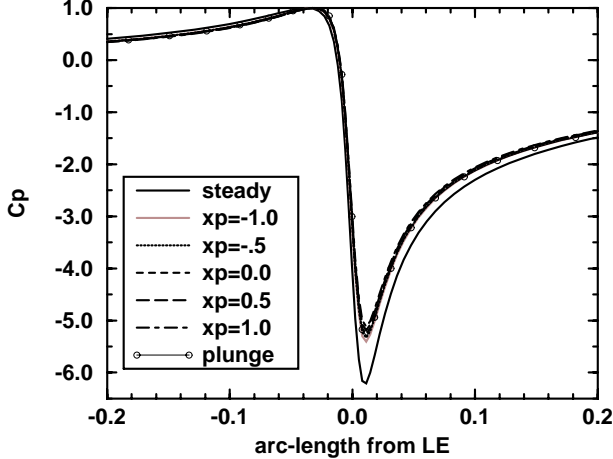


Fig. 7.  $C_p$  comparison for  $k = 0.1$  at  $\alpha = 10$ .

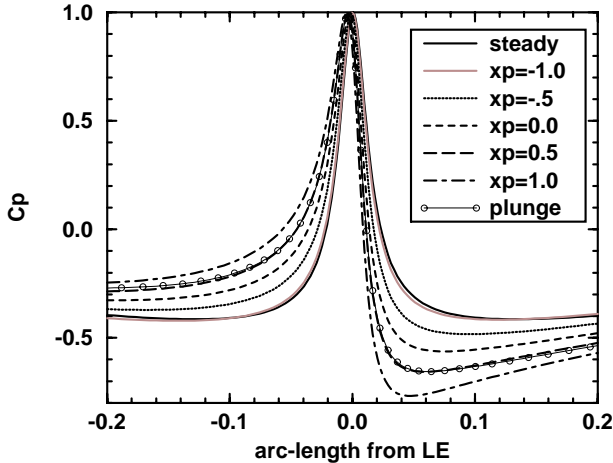


Fig. 8.  $C_p$  comparison for  $k = 0.1$  at  $\alpha = 0$   $\downarrow$ .

The results in Fig. 8 show a similar pressure distribution (near the LE) for an airfoil pitching about  $x_p = 0.5$  and an airfoil plunging with the same effective angle of attack. In contrast to Ericsson's theory, this shows agreement between pitching and plunging motions for  $\phi = 90$  degrees such that when  $\dot{\alpha}$  is maximum,  $\dot{z} = 0$  and  $\ddot{z}$  is minimum. However, this similarity is misleading, as pitching about the mid-chord introduces a coupled plunging motion.

Using a more robust approach for comparing the two motions, the pivot is fixed at the leading edge ( $x_p = 0$ ), such that there is no induced velocity at the leading edge due to the pitching motion, and then com-

parisons between the pressures at phase-angles other than 90 degrees are made. In Fig. 9 the pressure distribution near the leading edge for the airfoil in Fig. 8, pitching with  $x_p = 0$ , is compared with the same foil plunging with  $h = 1.76$  and phase-shifts of 93 and 94 degrees, that is, the pitching solution is at mid-stroke on the way up, at an angle of attack of zero degrees, and the plunging solutions are just past the top of the stroke at an effective angle of attack of roughly zero degrees.

Not surprisingly, comparisons of the lift coefficient time-histories also show a phase-shift of about 93 degrees. In Fig. 10 this is repeated for different reduced frequencies and the phase-shift (the phase-angle between the pitch and plunge motions required to yield lift-histories that are in-phase) is plotted as a function of the frequency.

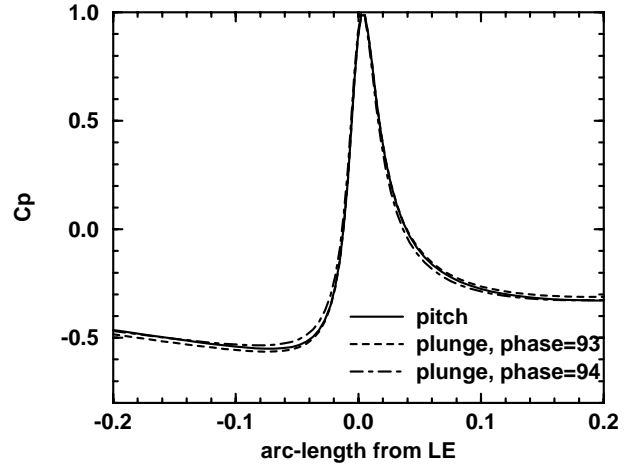


Fig. 9.  $C_p$  for pitching and plunging foils.

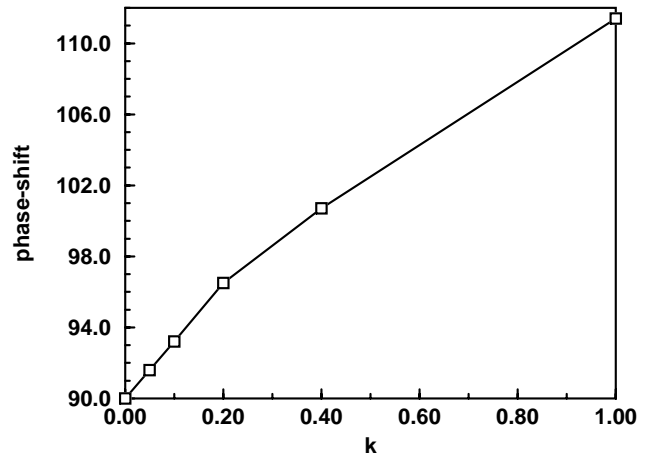


Fig. 10. Pitch/plunge phase-shift versus  $k$ .

The phase-shift appears to be relatively linear at very low frequencies where wake effects are small, and less linear at higher frequencies where wake-induced

nonlinearities become influential. The value at  $k = 0$  is a projected result, as a plunging simulation with  $k = 0$  is not easily performed.

From these results it is seen that the pressure distributions, and hence the resulting boundary layers, in the vicinity of the leading edge are similar for pitching and plunging airfoils if an appropriate phase-shift ( $\approx 90$  degrees) is considered. It is important to note that the similarity is limited to a small region near the leading edge, typically not beyond 10 or 20 percent of the chord length. However, since the formation of the separation bubble leading to dynamic stall on the NACA 0012 is usually well within this region, similar dynamic stall characteristics may be expected for pitching and plunging foils.

Past experimental and numerical results (Refs. 21 and 24) have shown a substantial delay in dynamic stall with increasing pitch rate. The panel code cannot reliably predict flows once separation has occurred, but it may be used to determine the angle of attack and airfoil position where laminar separation (indicating the likely formation of a separation bubble) first occurs. Here a NACA 0012 at a Reynolds number of  $10^6$  is pitched up from 0 to 20 degrees using the modified ramp (Eq. 10) with various pitch rates. In Fig. 11 the angle of attack where laminar separation is first predicted is plotted as a function of the reduced frequency.

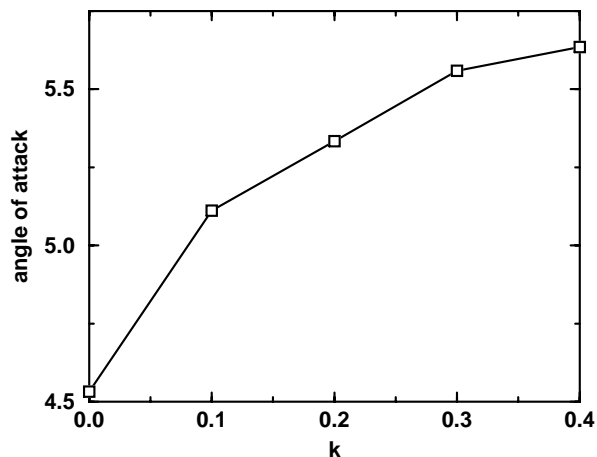


Fig. 11. Dynamic-stall onset angle of attack.

As expected, laminar separation is delayed as the pitch rate is increased, but interestingly the position of the stagnation point and the point of laminar separation remain constant. In fact, the pressure distribution (or the pressure gradient) at the angle of attack where laminar separation first occurs is virtually identical in each case, as shown in Fig. 12.

This means that the boundary layers will also be identical for each case. The identical pressure gradi-

ent distributions are in complete agreement with the Navier-Stokes simulations of Ref. 8, and the delay in dynamic stall onset is in qualitative agreement with the experimental results of Ref. 24. The experimental results could not predict the first stages of dynamic stall, but rather they visually determined dynamic stall by the appearance of a leading edge vortex in Schlieren photographs.

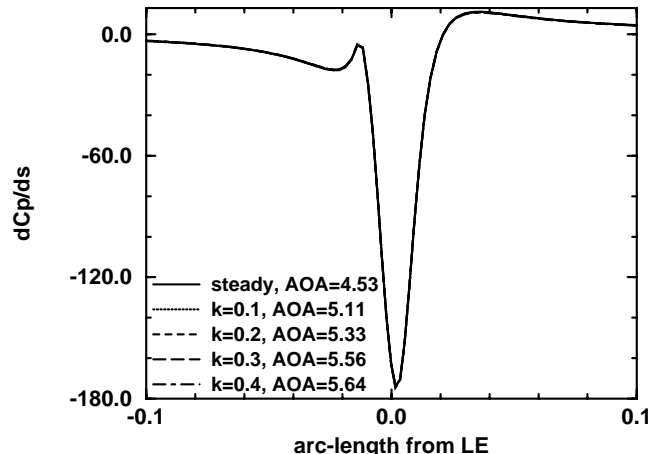


Fig. 12. Pressure gradient distribution at stall onset.

## Conclusions

An efficient computational approach was presented for the fast prediction of the onset of dynamic stall due to rapid incidence changes or due to pitch / plunge motions of blades or airfoils. The method provides a means for the systematic evaluation of flow properties leading to dynamic stall over a broad parameter space.

Presented results suggest that the primary factor in dynamic stall onset is the phase lag in the surface pressure, data that may be obtained to the point of separation using a purely inviscid analysis. Additionally, the ‘moving wall’ analogy for explaining the dynamic stall phenomenon is brought into question. Presented results demonstrate inadequacies in this theory.

Viscous results obtained from the hybrid code illustrate that the pressure lag effect delays flow separation in dynamic cases even at very low frequencies, and that the onset of dynamic stall occurs when a critical pressure gradient distribution is obtained. Furthermore, in agreement with previous Navier-Stokes simulations, the critical pressure distribution leading to dynamic stall was found to be independent of mode and frequency.

## Acknowledgments

This investigation was partially supported by the Naval Postgraduate School National Research Council Fellowship Program (KDJ) and the Naval Air Warfare Center, China Lake, California (MFP).

## References

- <sup>1</sup> Ericsson, L. E., "Moving Wall Effects in Unsteady Flow," **Journal of Aircraft**, Vol. 25, No. 11, Nov., 1988, pp. 977-990.
- <sup>2</sup> Tyler, J. C. and Leishman, J. G., "Analysis of Pitch and Plunge Effects on Unsteady Airfoil Behavior," **Journal of the American Helicopter Society**, July 1992, pp. 69-82.
- <sup>3</sup> Beddoes, T. S., "A Qualitative Discussion of Dynamic Stall," AGARD Special Course on Unsteady Aerodynamics, AGARD Report 679, 1979.
- <sup>4</sup> Dindar, M., Kaynak and U. Fuji, K., "Nonequilibrium Turbulence Modeling Studies on Light Dynamic Stall of a NACA 0012 Airfoil," AIAA Paper No. 90-3040, Aug. 1990.
- <sup>5</sup> Visbal, M. R., "On the Formation and Control of the Dynamic Stall Vortex on a Pitching Airfoil," AIAA Paper No. 91-0006, Jan. 1991.
- <sup>6</sup> Clarkson, J. D., Ekaterinaris, J. A. and Platzer, M. F., "Computational Investigation of Airfoil Stall Flutter," *Unsteady Aerodynamics, Aeronautics and Aeroelasticity of Turbomachines and Propellers*, Springer-Verlag, New York, 1993, pp. 415-432.
- <sup>7</sup> Ekaterinaris, J. A. and Platzer, M. F., "Numerical Investigation of Stall Flutter," ASME Paper No. 94-GT-206, 1994.
- <sup>8</sup> Grohsmeier, S. P., Ekaterinaris, J. A. and Platzer, M. F., "Numerical Investigation of the Effect of Leading Edge Geometry on Dynamic Stall of Airfoils," AIAA Paper No. 91-1798, June, 1991.
- <sup>9</sup> Teng, N. H., "The Development of a Computer Code for the Numerical Solution of Unsteady, Inviscid and Incompressible Flow over an Airfoil," Master's Thesis, Naval Postgraduate School, Monterey, CA, June 1987.
- <sup>10</sup> Hess, J. L. and Smith, A. M. O., "Calculation of Potential Flow about Arbitrary Bodies," **Progress in Aeronautical Sciences**, Vol. 8, pp. 1-138, Pergamon Press, Oxford, 1966.
- <sup>11</sup> Basu, B. C. and Hancock, G. J., "The Unsteady Motion of a Two-Dimensional Aerofoil in Incompressible Inviscid Flow," **Journal of Fluid Mechanics**, Vol. 87, 1978, pp. 159-168.
- <sup>12</sup> Platzer, M. F., Neace, K. S. and Pang, C. K., "Aerodynamic Analysis of Flapping Wing Propulsion," AIAA Paper No. 93-0484, Jan. 1993.
- <sup>13</sup> Riestler, P. J., "A Computational and Experimental Investigation of Incompressible Oscillatory Airfoil Flow and Flutter Problems," Master's Thesis, Naval Postgraduate School, Monterey, CA, June 1993.
- <sup>14</sup> Turner, M., "A Computational Investigation of Wake-Induced Airfoil Flutter in Incompressible Flow and Active Flutter Control," Master's Thesis, Naval Postgraduate School, Monterey, CA, March, 1994.
- <sup>15</sup> Tuncer, I. H., Platzer, M. F. and Ekaterinaris, J. A., "Computational Analysis of Flapping Airfoil Aerodynamics," ASME Fluids Engineering Division, Summer Meeting, June, 1994.
- <sup>16</sup> Jones, K. D. and Platzer, M. F., "Time-Domain Aeroelastic Analysis of a two Airfoil System with Application to Unsteady Rotary Wing Flowfields," AIAA Paper No. 95-0337, Jan., 1995.
- <sup>17</sup> Jones, K. D., Dohring, C. M. and Platzer, M. P., "Wake Structures Behind Plunging Airfoils: A Comparison of Numerical and Experimental Results," AIAA Paper No. 96-0078, Jan., 1996.
- <sup>18</sup> Keller, H. B. and Cebeci, T., "Accurate Numerical Methods for Boundary-Layer Flows, pt. 2, Two-Dimensional Turbulent Flows," **AIAA Journal**, Vol. 10, p. 1193, 1972.
- <sup>19</sup> Nowak, L. M., "Computational Investigations of a NACA 0012 Airfoil in Low Reynolds Number Flows," Master's Thesis, Naval Postgraduate School, Monterey, CA, Sept., 1992.
- <sup>20</sup> Cebeci, T., "Essential Ingredients of a Method for Low Reynolds-Number Airfoils," **AIAA Journal**, Vol. 27, No. 12, Dec., 1989, pp. 1680-1688.
- <sup>21</sup> VanDyken, R. D., Ekaterinaris, J. A., Chandrasekhara, M. S. and Platzer, M. F., "Analysis of Compressible Light Dynamic Stall Flow at Transitional Reynolds Numbers," **AIAA Journal**, Vol. 34, No. 7, July, 1996, pp. 1420-1427.
- <sup>22</sup> Hancock, G. J. and Mabey, D. G., "Unsteady Aerodynamics of Controls," AGARD CP-465, April, 1990.
- <sup>23</sup> Cebeci, T., Platzer, M. F., Jang, H. M. and Chen, H. H., "An Inviscid-Viscous Interaction Approach to the Calculation of Dynamic Stall Initiation on Airfoils," **Journal of Turbomachinery**, Vol. 115, No. 4, Oct., 1993, pp. 714-723.
- <sup>24</sup> Chandrasekhara, M., Ahmed, S., and Carr, L., "Schlieren Studies of Compressibility Effects of Dynamic Stall of Airfoils in Transient Pitching Motion," AIAA Paper No. 90-3038, Aug. 1990.